



Article

Medium-Range Aircraft Conceptual Design from a Local Air Quality and Climate Change Viewpoint

Karim Abu Salem ^{*}, Giuseppe Palaia , Alessandro A. Quarta  and Mario R. Chiarelli 

Department of Civil and Industrial Engineering, University of Pisa, Via G. Caruso 8, 56122 Pisa, Italy; giuseppe.palaia@phd.unipi.it (G.P.); alessandro.antonio.quarta@unipi.it (A.A.Q.); mario.rosario.chiarelli@unipi.it (M.R.C.)

* Correspondence: karim.abusalem@ing.unipi.it

Abstract: This paper presents an overall performance assessment of hybrid-electric medium-range transport aircraft, with the aim to evaluate the potential of such a propulsion technology towards the reduction in the environmental impact of aviation transport, in terms of both local air quality degradation in airport areas and climate change. The proposed approach presents distinct analyses of the environmental impact of transport aircraft, distinguishing climate-changing effects from local pollution effects so that the integration of hybrid-electric propulsion is carried out to face the two issues specifically. The proposed analysis, although of conceptual nature, presents a clear scenario in which, given the technological limitations of batteries, the use of hybrid-electric propulsion on medium-haul aircraft can only be useful to reduce local pollution. In contrast, other solutions are needed to mitigate the climate-changing impact.

Keywords: aircraft conceptual design; hybrid-electric aircraft; local air quality; climate change; aircraft emissions



Citation: Abu Salem, K.; Palaia, G.; Quarta, A.A.; Chiarelli, M.R. Medium-Range Aircraft Conceptual Design from a Local Air Quality and Climate Change Viewpoint. *Energies* **2023**, *16*, 4013. <https://doi.org/10.3390/en16104013>

Academic Editor: Emilio Larrodé

Received: 19 April 2023

Revised: 4 May 2023

Accepted: 9 May 2023

Published: 10 May 2023



Copyright: © 2023 by the authors. Licensee MDPI, Basel, Switzerland. This article is an open access article distributed under the terms and conditions of the Creative Commons Attribution (CC BY) license (<https://creativecommons.org/licenses/by/4.0/>).

1. Introduction

Significant contributions to air pollution and climate change are provided by aviation transport [1]. The issue of the environmental impact of aircraft operations has gained more significance as the effects of both carbon dioxide (CO₂) and non-CO₂ emissions on society and the environment are becoming increasingly crucial. Therefore, currently, one of the main objectives of aviation research is to reduce aircraft (atmospheric) emissions, whose impact can be investigated at different levels, from the degradation of the local air quality to the impact on climate change.

The local air quality mainly refers to the level of air pollution in the areas surrounding the airports, below the altitude of 915 metres above ground level [1], so that reducing local air pollution may have a significant impact on the quality of life and health of citizens, as polluting emissions related to aircraft operations have a direct correlation with respiratory and cardiovascular diseases with associated premature deaths [2]. In order to improve local air quality, it is necessary to focus on technological developments which reduce emissions of non-CO₂ pollutants, such as nitrogen oxides (NO_x), sulphur oxides (SO_x), volatile organic compounds (VOC), and particulate matter (PM), mainly during taxiing, take-off, and initial climb, approach, and landing.

The impact of aviation on global climate change, on the other hand, has different characteristics. In fact, CO₂ emissions have a predominant contribution, especially on long-time scale effects, while non-CO₂ emissions have a non-negligible impact on short-term effects [3]. The social and environmental effects of climate change are different from those of local air pollution, as climate change involves large-scale effects, such as severe localised meteorological events, rising sea levels, disruption of ecosystems, forced migrations, and desertification.

This short overview suggests that the impact of aviation can be divided into two main categories with different origins, causes, and effects. In particular, to improve local air quality, it is necessary to introduce technological and operational solutions capable of cutting pollutant emissions in the so-called Landing and Take-Off cycle (LTO) [4], where non-CO₂ emissions performs a prevalent role. On the other hand, tackling climate-changing effects requires a general reduction in direct emissions through the entire aircraft-based operating cycle.

In this work, the challenges of reducing this two-fold environmental impact are addressed with the assessment of the hybrid-electric propulsion systems [5] integrated into the short-medium range (SMR) aircraft. In fact, using electric power could be a promising solution to reduce direct emissions and a complete review of the potential of such a specific technology is detailed in Ref. [6]. The integration of electric power systems into transport aircraft is constrained by the technological maturity of the batteries, as the low gravimetric energy density of this important component currently constitutes a strong limitation. In this work, the energy density of batteries has been selected in agreement with the next decade's forecasts [7]. As the problems of local air quality degradation and climate change have different causes and effects, two different strategies of electric power integration are evaluated to face the two problems separately. The first strategy, devoted to the minimisation of air pollution, involves an electric power retrofitting of the propulsion system of a baseline short-medium range aircraft. Such a particular strategy is based on a partial utilisation of electric power, limited to the LTO phase, and aiming to cut emissions close to airport areas. The second strategy aims to assess the potential of hybrid-electric propulsion towards the minimisation of aircraft greenhouse emissions. In that case, a complete redesign of both the aircraft and propulsion system is provided to minimise the block fuel consumption throughout the entire mission, where the block fuel is the fuel actually burned during aircraft standard operations and thus does not include the amounts related to diversion and reserves. A summary of this methodological structure is reassumed in Table 1.

Table 1. Aircraft implication with local air quality and climate change.

	Local Air Quality	Climate Change
Mission phase	LTO cycle	Entire mission
Impactful emissions	NO _x , SO _x , VOC, PM	CO ₂ , NO _x , water vapour, soot particles
Space-scale	Airport regions	Global effects
Effects	Direct damage to health	Large-scale effects, catastrophic implications
Proposed solution	Hybrid-electric propulsion retrofit for LTO emission suppression	Hybrid-electric aircraft redesign for block fuel minimisation

Given the duality of the problem and the related approaches, once the models used for the proposed analyses have been defined, the structure of the paper is conceptually divided into two branches; the details of the issue, the background, the proposed solution, and the findings are defined specifically first for the local air quality, then for climate change.

Several studies have already presented the integration of hybrid-electric propulsion on commercial aircraft, focusing on different transport categories. Given the weight penalties of batteries, the most tangible applications for initial effective integration of power electrification are related to small aircraft. The design and performance of electric or hybrid-electric general aviation [8,9] and commuter aircraft [10–12] have been widely evaluated. Conceptual studies have also presented novel electric aero-taxi [13,14] in the future context of urban air mobility. Moving on to larger aircraft, several studies involved the regional category [15–18], which seems to be the most realistically compatible for effective integration of electric propulsion in the next decade [19]. Many concerns, however, remain about the application of such propulsion on larger aircraft, as the short-medium range.

The severe weight penalties associated with the installation of battery packs could make power electrification unlikely for this aircraft class [6]. Nevertheless, as these aircraft are the most used [20], contributing to a large share of aviation's emissions [21], an investigation into the potential of power electrification on SMR aircraft is at least necessary. In this regard, some conceptual studies have already investigated the performance potential of hybrid and electric SMR aircraft [22–24]; however, values of battery energy densities larger than that forecasted in the technical literature are generally adopted in these works, or no gains, in terms of environmental benefits, are achieved. In this paper, on the other hand, starting with the use of a battery technology value compatible with predictions for 2035, the potential of hybrid-electric propulsion on SMR aircraft is assessed by moving from a general to a particular analysis. Therefore, the potential benefits of power electrification are not only assessed in general terms of reducing fuel consumption but also analysing how ground air pollution can be reduced.

The preliminary results obtained show that the introduction of hybrid-electric propulsion on SMR aircraft allows to eliminate direct emissions in airport areas, providing a viable solution for local air quality improvement. Conversely, the approach aiming at minimising fuel consumption throughout the entire aircraft mission leads to poor solutions in terms of the actual potential of drastically reducing the climate-changing footprint of this class of aircraft. These outcomes provide a further building block in the ongoing research regarding the reduction in the environmental impact of transport aircraft. Although of a conceptual nature, this study clearly outlines the limits and potential of the application of hybrid-electric propulsion to SMR aircraft, providing insights for future technical developments on the one hand and clarifying the lack of benefits on the other.

This paper is organised as follows: Section 2 introduces the methodologies and the tools used to perform the designs and related performance analyses; Section 3 focuses on the problem of local air pollution, defining the problem and the proposed retrofit solution; and Section 4 moves to the climate change issue, defining its implications and the re-design strategy proposed to address it. Finally, Section 5 summarises the outcomes obtained in this research.

2. Materials and Methods

2.1. The Baseline Short-Medium Range Aircraft

The reference aircraft selected for this study is the CeRAS CSR-01 [25] which is a virtual representation of the well-known Airbus A320. The CeRAS open database [26] allows the research community to use this common standard reference for aeronautic research projects. Specifically, this platform is very useful for performing comparative studies relating to the introduction of new aircraft technologies, as discussed in [27] for the assessment of an innovative airframe. A three-view of the CeRAS CSR-01 is represented in Figure 1.

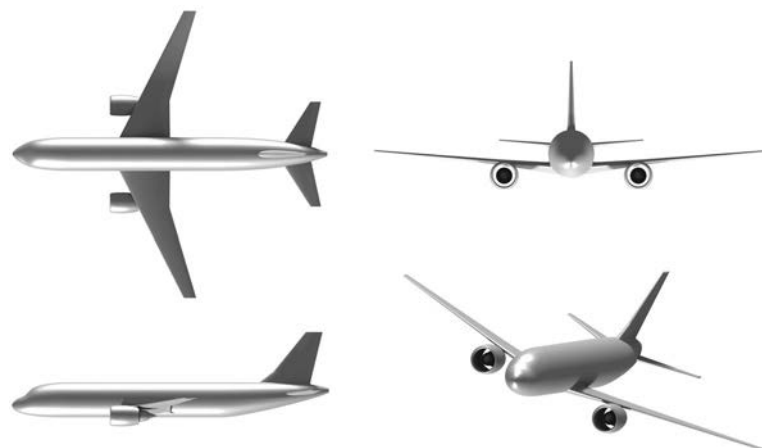


Figure 1. Sketch of the CeRAS CSR-01 aircraft.

In this work, only the geometrical features have been extracted from the public CeRAS database, while the aerodynamic assessment, the weights estimation, and the overall performance evaluations have been made by means of specific tools, which are described in Section 2.2.

2.2. Hybrid-Electric Aircraft Design Methodology

An in-house developed environment for the conceptual design and performance analysis of hybrid-electric aircraft has been used in this study. This tool, named THEA-CODE (*'Tool for Hybrid-Electric Aircraft Conceptual Design'*) and first conceived to study regional hybrid aircraft [28], has been applied in this research to design short-medium range hybrid-electric aircraft. The tool performs aircraft sizing by means of an iterative design workflow (Figure 3), briefly detailed in the following. First, in the *Aerodynamic evaluations* block, the Vortex Lattice Method (VLM) code named Athena Vortex Lattice (AVL) [29] is used to evaluate trim, stability, and induced drag, whereas the consolidated literature methods are used to evaluate the parasitic [30] and wave drag [31]. Furthermore, if higher fidelity datasets are available, it is possible to use these data to perform more detailed aerodynamic evaluations, e.g., outcomes from CFD-based tools for aerodynamics assessments [32,33] or CFD-built databases [34,35] can be integrated in the design workflow to replace VLM and textbook methods evaluations. The *Propulsion system sizing* stage performs the sizing of thermal engines and electric motors by using the matching chart shown in Figure 2, which is a diagram that correlates the required specific power (P/W) with the aircraft wing loading (W/S) [36,37]. The requirements for the specific power to be installed on board are provided by [38]; from this graph is also possible to visualise the power split between thermal and electric installed power.

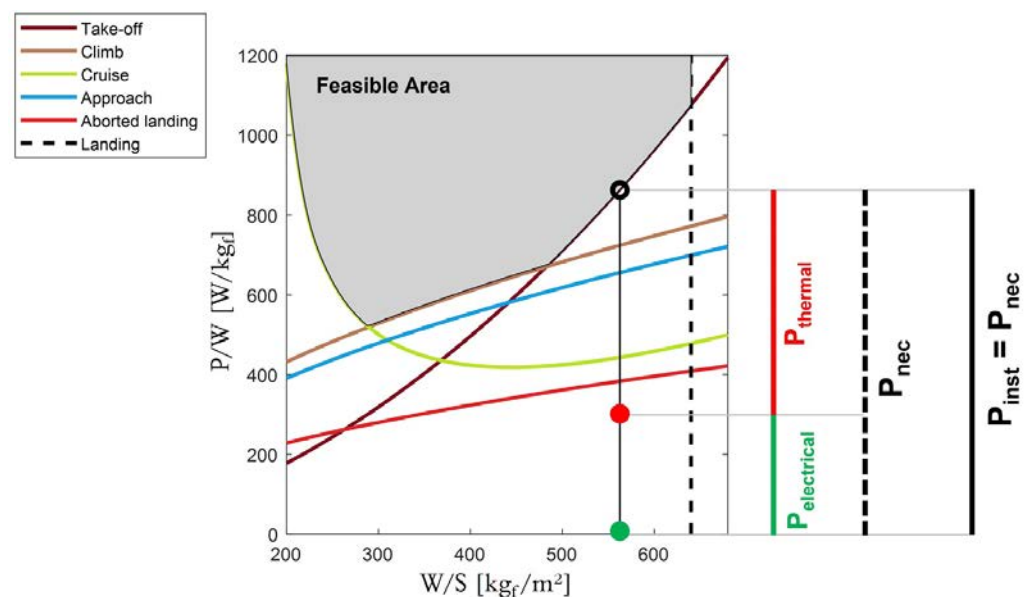


Figure 2. Example of matching chart for a parallel hybrid-electric powertrain.

The phases considered are take-off, climb with one engine inoperative, cruise, approach climb, and aborted landing. The relationships derived for each phase are based on the following assumptions: (i) the aircraft has been considered as a point mass; (ii) the aircraft's polar drag has been computed according to the method described in *Aerodynamic evaluations*; (iii) in case of landing gear or flap/slat extracted, the aircraft's polar drag has been computed adding their contribution as described in [37,39]; and (iv) efficiency of electric components is assumed constant for each phase. According to the above hypotheses and using the classical approach to evaluate the performance of the considered flight

phases, the specific power constraints derived are reported in Equations (1)–(4), which are consistent with the mathematical model discussed in Appendix A and Ref. [19].

$$\left(\frac{P}{W}\right)_{TO} \geq \left(\mu_{TO} + \frac{\frac{k_{VR}^2 (C_D - \mu_{TO} C_L)}{C_{Lmax}}}{1 - e^{-\rho g (C_D - \mu_{TO} C_L) (\frac{l_{TO}}{\phi} - S_R - S_{LO}) / (W/S)}}\right) \sqrt{\frac{2(W/S) k_{V2}}{\rho C_{Lmax} \eta_P}} \quad (1)$$

$$\left(\frac{P}{W}\right)_{CL_i} \geq \frac{\left(\frac{q C_{Di} V_i}{W/S} + \gamma_i V_i\right)}{k_e \eta_P} \quad (2)$$

$$\left(\frac{P}{W}\right)_{CR} \geq \frac{q C_D V}{(W/S) \eta_P} \quad (3)$$

$$\left(\frac{P}{W}\right)_{APP} \geq \frac{q C_D V}{k_e (W/S) \eta_P} + \frac{V \gamma}{k_e \eta_P} \quad (4)$$

Equation (1) relates to the take-off power requirement and shows that higher values of wing loading are associated with higher values of specific power. In fact, if wing loading increases, stall speed rises as well, and, consequently, more power is necessary to accomplish take-off in a fixed runway length set by the Top Level Aircraft Requirements (TLAR). A similar trend occurs for Equations (2) and (4), which are related to the climb phase with one engine inoperative, and aborted approach or landing (approach climb), respectively. Cruise phase specific power constraint, described by Equation (3), is related to the equilibrium in level and steady flight. In this case, an optimum wing loading exists, which corresponds to the maximum lift-to-drag ratio of the configuration, so the value of the optimum wing loading is strictly related to the aircraft’s aerodynamic design.

The envelope of the constraints defines a feasible region (grey area of Figure 2), and its lower border identifies the locus of the minimum specific powers for each wing loading considered. Consequently, the installed specific power, $\left(\frac{P}{W}\right)_i$, is evaluated according to Equation (5):

$$\left(\frac{P}{W}\right)_i = \max \left\{ \left(\frac{P}{W}\right)_{TO}, \left(\frac{P}{W}\right)_{CL_i}, \left(\frac{P}{W}\right)_{CR}, \left(\frac{P}{W}\right)_{AC}, \left(\frac{P}{W}\right)_{LC} \right\} \quad (5)$$

In the *Mission analysis* block of the design workflow, a time-marching simulation of the reference mission is carried out according to the indications and methods given in [40,41]. In this context, the mission is split in taxi-out, take-off, climb, cruise, descent, climb-to-alternate, cruise-to-alternate, descent, loiter, approach, landing, and taxi-in. For each time-step, the aircraft’s point-mass equations of motion, detailed in Equation (6), are time integrated to evaluate cinematic and performance, taking aerodynamics and weights (evaluated in the other blocks of the workflow) into account.

$$\begin{cases} \frac{dW}{dt} = -C_t P^t \eta_{tc} / V \\ L = W \\ P = DV + \gamma VW \\ P^t \eta_{tc} + P_b \eta_{ec} = P \\ P^t = \Phi^t P_i^t \end{cases} \quad (6)$$

where W is the aircraft weight, C_t is the thrust specific fuel consumption, L and D are aircraft lift and drag forces, respectively; P is the power requested to complete each considered flight stage; γ is the trajectory slope; P^t and P_b are the power supplied by the thermal

engine and the battery pack, respectively; η_{tc} and η_{ec} are the thermal and electric chain efficiency, respectively; Φ^t is the power fraction supplied by the thermal engine; and P_i^t is the installed thermal engine power. The primary outputs of the simulation are the fuel consumption and/or the required battery mass; a comprehensive description of the mission simulation analysis for hybrid-electric aircraft is given in [16]. Finally, in the *Aircraft weights estimation* block, the total weight of the aircraft is computed considering the payload weight (provided as input), the fuel and battery weight (provided by the mission analysis module) and the operative empty weight, evaluated according to the methodology present in [42].

The design procedure is initialised by providing, as input a set of TLAR, information on the technological level of the electrical machines and batteries, and a starting geometry. THEA-CODE sizing procedure ends once convergence on the maximum take-off weight is reached. Since the detailed description of the code is beyond the scope of this paper, for more details, the interested can refer to [19,28]. Note that the THEA-CODE (Figure 3) is not conceived to modify and/or optimise the geometry of the aircraft, but it can only homothetically scale an input baseline geometry. In fact, THEA-CODE has been developed to work synergically with the aerodynamic optimiser AEROSTATE [43], specifically developed to optimise aircraft geometry.

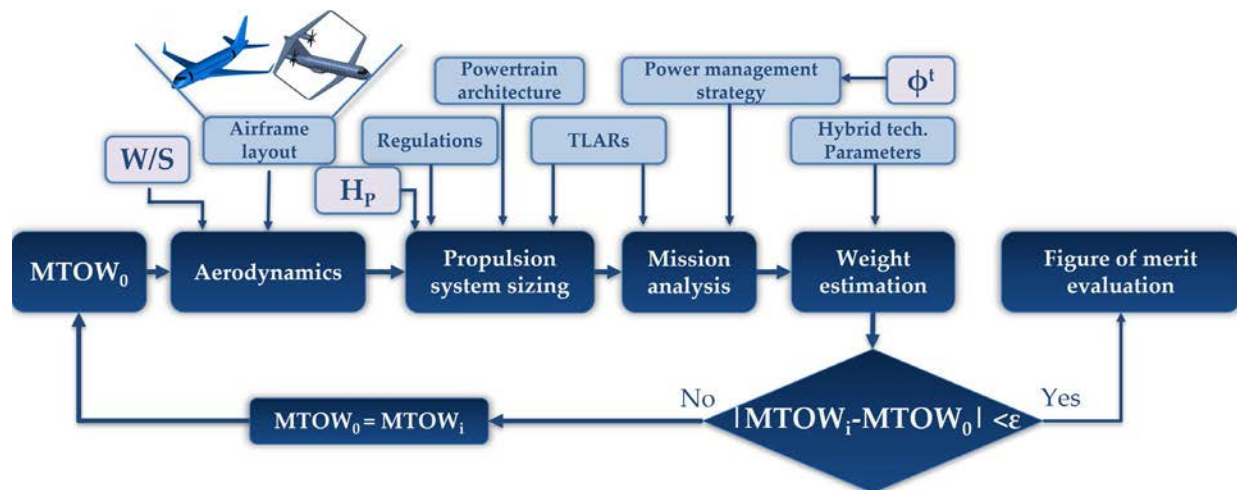


Figure 3. Simplified scheme of the THEA-CODE iterative workflow.

2.3. Common Assumptions

The parameters related to the technology level of the electrical machines and batteries used in this conceptual study, taking into account the forecasts for a possible aircraft entry into service in 2035, are:

- The hybrid-electric powertrain architecture is assumed to be parallel; the integration of the two power units, at this conceptual stage, is assumed according to the scheme proposed in [44]. Specifically, the electric motor is directly connected to the low-pressure shaft of the engine; this solution avoids the need for a gearbox. Furthermore, the electric motor is located in the cold section of the engine, reducing the risks of overheating [44]. This architecture allows to simultaneously supply power to the fan from both the thermal and electrical sources, so that the two power sources can supply power in different shares during each mission timestep;
- The battery energy density (BED) @pack level is assumed equal to 500 Wh/kg [45];
- The electric motor power density is assumed to be equal to 15 kW/kg [45];
- The electric power cable density per linear meter is assumed equal to 6.5 kg/m [44].

3. Retrofit Strategy towards the Improvement of Local Air Quality

3.1. Local Air Quality

Transport aircraft operations have increased with high growth rates over the past decades [46] and the trend is expected to continue [47]. This led to an increase in traffic at airports, which have often been overloaded or saturated [48]. Aircraft engines produce a variety of pollutants, such as NO_x, CO, hydrocarbons (HC), sulphur dioxide (SO₂), and PM. Several studies have shown that air pollutants produced by ground air traffic at large airports can affect the air quality in the airport's surrounding region [49,50]. Millions of people live in the vicinity of airports and, therefore, are regularly exposed to this air pollution, which may cause adverse health consequences [51,52]. Increases in cardiovascular, respiratory, and hypertension diseases have been observed near airport areas [53,54]; consequently, there have been reported incremental trends in premature deaths [2]. Studies on these pathologies have led to the fact that the most dangerous pollutants include PM [49,55]. The impact of aircraft operations on the concentration of these pollutants in areas around airports has been shown to be predominant [49,56]; these occur mainly in the LTO cycle. In [2,49], it is shown that the highest PM and NO_x emissions derive from high-thrust engine operating modes, such as take-off and climb-out, whereas HC and CO emissions are mainly attributable to low-thrust phases, such as taxiing. These results are important for establishing strategies to tackle the problem of air quality degradation. For example, ref. [55] suggests that the use of a single engine for the taxiing phases does not reduce PM and NO_x emissions but may be useful for lowering CO and HC emissions. The same conclusions would be reached with the implementation of electrical systems for the ground handling of aircraft during taxiing [57]. However, these solutions are partial and probably of minor overall impact [55], whereas a breakthrough change is necessary to achieve a thorough reduction in air pollution in airport areas. For this reason, this study focuses on the integration of hybrid-electric propulsion for SMR aircraft to perform the entire LTO cycle with electric power exclusively. In this way, all direct pollutant emissions from aircraft operations would be eliminated.

3.2. Retrofit Procedure

The first strategy to integrate electric propulsion within the SMR aircraft is a retrofit of the baseline aircraft. With this procedure, only the propulsion system of the aircraft is re-designed, whereas the external shape and primary structure are kept unvaried. This has the advantage of allowing for an agile and flexible reconfiguration of a given aircraft, but it has the disadvantage of leaving no room for architectural modifications. Since the shape of the aircraft is the same, also aerodynamic performance is not different; for this study, the aerodynamic database produced by means of CFD RANS solver in [41] for the CeRAS CSR-01 has been used to carry out the aerodynamic evaluations. In a retrofitting procedure, constraints related to the baseline aircraft must be taken into account; the main constraint is to verify the compliance with the Maximum Take-Off Weight (MTOW) of the baseline. Indeed, the main structure of the baseline, which is kept unvaried, is sized according to this MTOW. Furthermore, there are some components whose weight does not vary with respect to the baseline during the retrofit. Specifically, the overall structural weight (including wing, fuselage, and landing gear) and the onboard systems are fixed weights. Instead, the weight of other items can differ from the baseline; among these, there is the weight of the propulsion system, which is totally re-designed, and the weights of the operational items related to the number of passengers; indeed, the retrofit procedure proposed in this study includes the possibility of varying the maximum number of passengers. The weights of the payload-related items, such as cabin furnishing, are therefore re-evaluated for each configuration considered.

There are already other case studies in the literature regarding hybrid-electric retrofit of transport aircraft [58–60]. However, these were primarily aimed at reducing the general environmental impact of the aircraft, attempting to reduce overall fuel consumption. In this study, instead, the objective of hybrid-electric retrofitting is to suppress polluting

emissions in the proximity of airport areas, thus reducing local pollution. This has a direct impact on the retrofitting procedure, mainly on the sizing constraints of the propulsion system and on the split of installed power between the thermal and electrical chains. Specifically, it is imposed to perform the LTO cycle with the exclusive use of electric power; this strategy totally avoids the use of thermal engines for standard LTO operations and therefore eliminates noxious emissions in airport surroundings. All the other flight phases, i.e., climb, cruise, descent, diversion, and loiter, are accomplished with the sole use of thermal power. Figure 4 sketches the power utilisation strategy for the retrofitted SMR aircraft.

mission phase	power utilization strategy
taxi-out	full electric
take-off	full electric
climb	full thermal
cruise	full thermal
descent	full thermal
diversion	full thermal
loiter	full thermal
landing	full electric
taxi-in	full electric

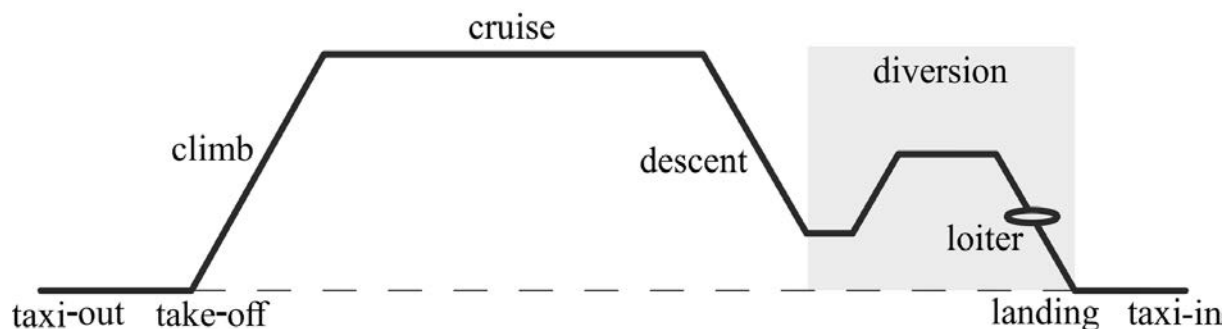


Figure 4. Power split and supply strategy for the retrofit procedure.

Given this power supply strategy, the propulsion system is sized as follows: the electric motors are sized to meet the take-off requirement; the thermal engines are subjected to the most restrictive constraint of the whole matching chart. Consequently, the matching chart is split into two parts: one relevant to the electric propulsion sizing (Figure 5-left) and one related to the requirements on thermal specific power (Figure 5-right). Electric installed power and thermal installed power are evaluated according to Equations (7) and (8), respectively:

$$\left(\frac{P}{W}\right)_i^e = \left(\frac{P}{W}\right)_{TO} \quad (7)$$

$$\left(\frac{P}{W}\right)_i^t = \max\left(\left(\frac{P}{W}\right)_{CL_i}, \left(\frac{P}{W}\right)_{CR}, \left(\frac{P}{W}\right)_{AC}, \left(\frac{P}{W}\right)_{LC}\right) \quad (8)$$

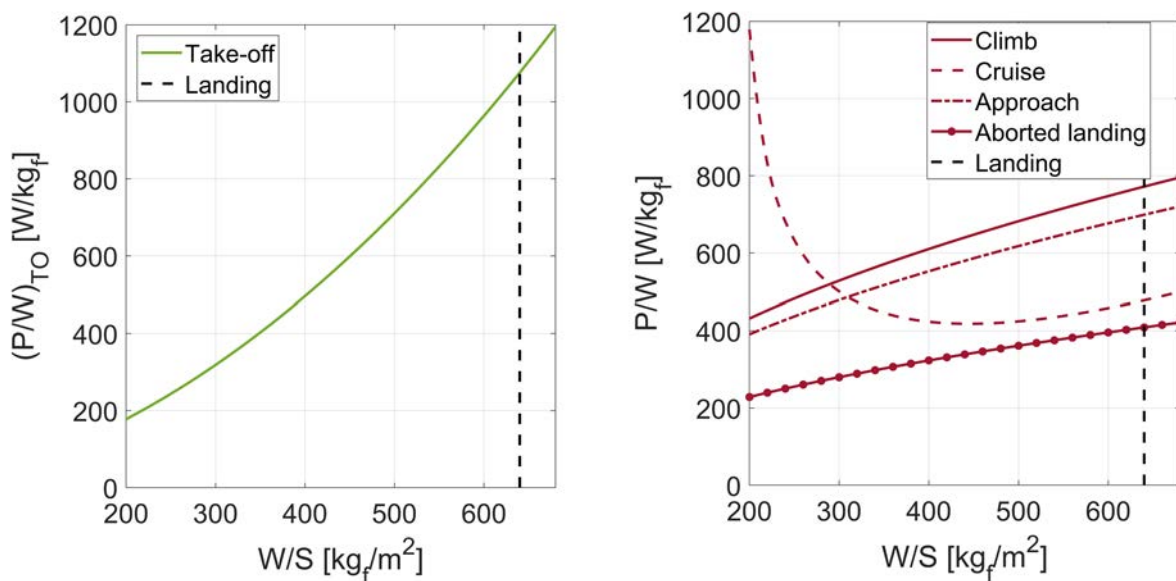


Figure 5. Qualitative matching charts for the retrofit strategy: electric (left) and thermal (right) specific power.

3.3. Retrofit Results

Sensitivity studies have been conducted involving two main design requirements for a transport aircraft: number of passengers and flight distance. Other requirements, such as runway length, cruise speed and altitude, are left fixed to those of the baseline aircraft [41].

The sensitivity analyses have been performed by varying the number of passengers between 80 and 186 and the flight distance between 1000 and 4800 km; the latter value represents the harmonic range of the baseline [41]. Sensitivity studies have been completed in two steps:

- In the first step, called the *design phase*, the baseline aircraft is retrofitted for each pair of values of number of passengers and flight distance considered (according to the workflow of Figure 3). For example, an aircraft with a number of passengers equal to 115 and a flight distance equal to 2000 km will have a cabin reconfigured with 115 seats equal and a harmonic range of 2000 km. The hybrid propulsion system is sized to meet the power requirements for this specific design point. For the considered design point, the take-off weight W_{TO} calculated within the retrofitting procedure corresponds to its MTOW; this is always lower than the MTOW of the baseline.
- In a second step, called the *analysis phase*, representative configurations are selected from those evaluated in the *design phase*, and the performance within their allowable payload-range envelope is evaluated.

First, the results of the *design phase* are proposed in the shape of maps at varying design points (i.e., passengers and range). All the feasible configurations obtained with the retrofit procedure have LTO fuel = 0 kg, as they are able to perform the LTO cycle with only electric power. Figure 6 shows the values of battery mass m_b (left) and block fuel mass m_{fb} (right), provided by the *Mission analysis* module of the workflow described in Section 2.2. As might be expected, both battery mass and fuel needed for the mission increase as the number of passengers and range increase. The battery mass, which is used only in LTO phases, is mainly needed for the take-off, which requires the supply of maximum electrical power. The trend of the contour lines of the m_b is in agreement with the trend of the maximum take-off weight of the retrofitted configurations, whose map is shown in Figure 7-left. In fact, the installed electrical power (Figure 9-right) is constrained by the take-off power requirement, which depends mainly on the take-off mass of the aircraft. The trend is different for the block fuel (Figure 6-right); the effect of range variation

is much more pronounced than that of the payload: fuel consumption is predominant in the cruise phase, and the distance travelled has a major impact on consumption.

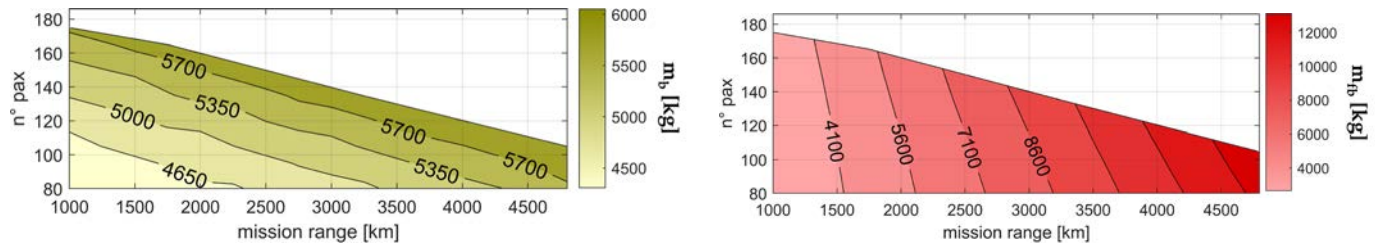


Figure 6. Battery mass (left) and block fuel mass (right).

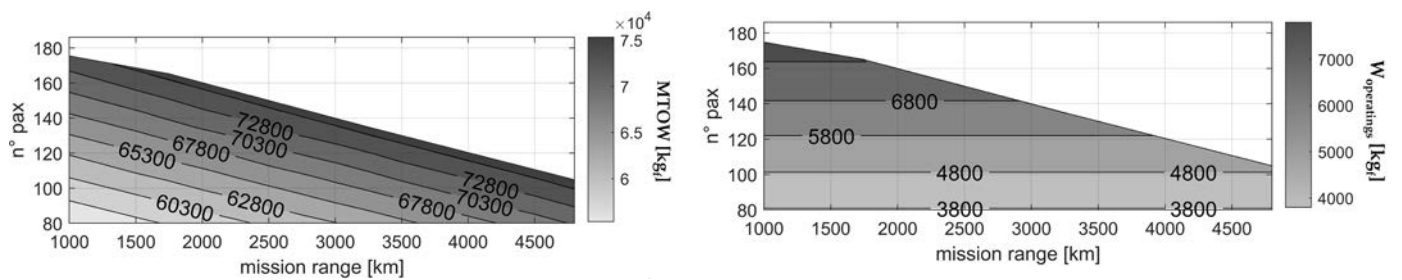


Figure 7. MTOW (left) and operating items (right) weights.

Figure 7-left shows the maximum take-off weight trend for each retrofitted configuration. There is an unfeasible area of the payload-range envelope (the white area of the charts), which, instead, is admissible for the baseline aircraft [41]. This is due to the larger operating empty weight of the retrofitted configurations caused by the on-board installation of electric machines and batteries; the constraint on $MTOW_{MAX}$ must be respected for each retrofitted design, hence this results in a contraction of the payload-range design space. On the other hand, part of the weight increase due to batteries is slightly compensated by a reduction in the weights of operating items related to the number of passengers (seats, furnishings, galleys, crew, toilet, etc.), as shown in Figure 7-right.

Figures 8 and 9 show the results of specific power $P/MTOW$ and installed power P , respectively. The results are given in terms of requested power to the whole powertrain (left), to the thermal part (centre), and to the electrical part (right).

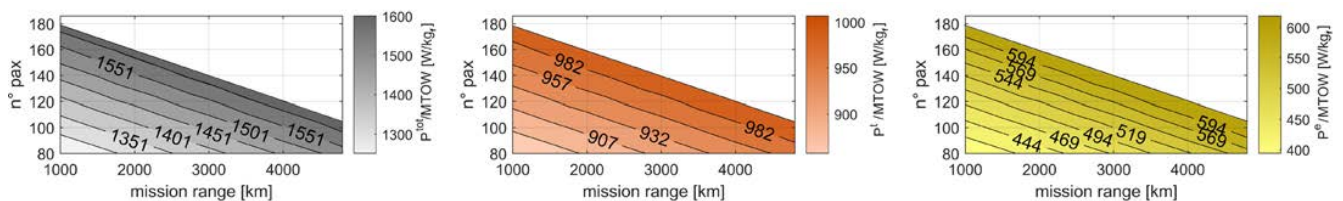


Figure 8. Specific power: total (left), thermal (centre), and electric (right).

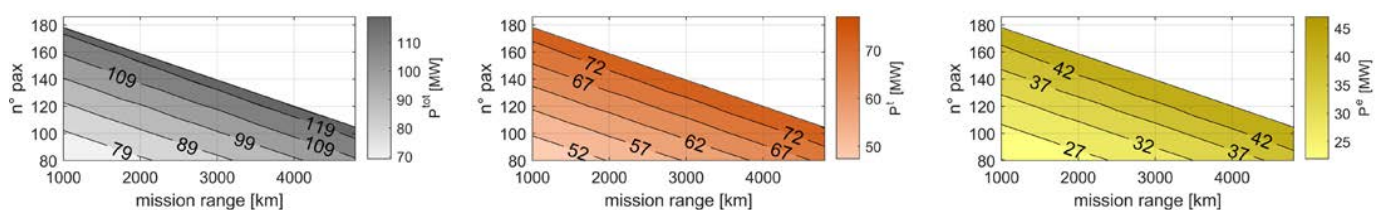


Figure 9. Installed power: total (left), thermal (centre), electric (right).

As mentioned in Section 3, the sizing requirement for electric propulsion is related to take-off; on the other hand, the thermal power, in these case studies, is related to the

climb. The requested specific power for both thermal and electrical chains decreases as the payload and/or range decreases and, therefore, as the MTOW decreases. Since the wing reference surface is the same for each retrofitted configuration, as the take-off weight decreases, there is a corresponding reduction in wing loading W/S (Figure 10). Wing loading is a fundamental variable in the evaluation of the specific power required during take-off and climb. Therefore, as W/S decreases, there is a beneficial reduction in the required specific power and, consequently, in the total installed power (Figures 8 and 9).

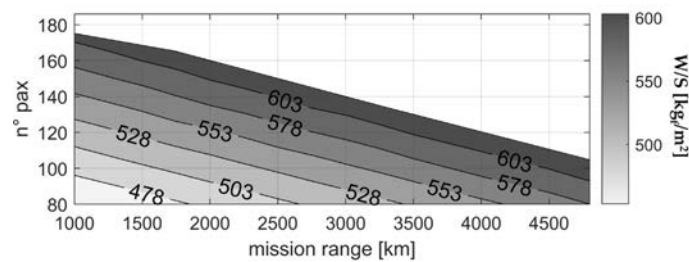


Figure 10. Wing loading varying mission range and number of passengers onboard.

In the subsequent *analysis phase*, two different configurations obtained in the *design phase* are analysed: one sized to have a number of passengers equal to 120 and a design range equal to 2000 km, named *Configuration 1*, and one with a number of passengers equal to 174 and a design range equal to 1500 km, named *Configuration 2*. Differently for the *design phase*, the results are proposed in the shape of maps inside the actual payload-range envelope of the considered configuration. Figure 11a shows the trend of the take-off weight (W_{TO}) for the two configurations, whose MTOWs are shown in Figure 11b. The MTOW of *Configuration 1* is 67,100 kg, whereas that of *Configuration 2* is 76,800 kg. The differences between the two configurations lie mainly in the following:

1. Propulsion system masses, both thermal and electrical, due to the differences in power requirements. *Configuration 1* has a lower specific power requirement (Figure 12-right) due to the lower wing loading; furthermore, the lower MTOW implies a reduction in the total installed power (Figure 12-left);
2. Operating mass, which mainly depends on the number of passengers;
3. Fuel and battery mass required at the design point;
4. Take-off weight;
5. Mass breakdown of *Configurations 1* and *2*.

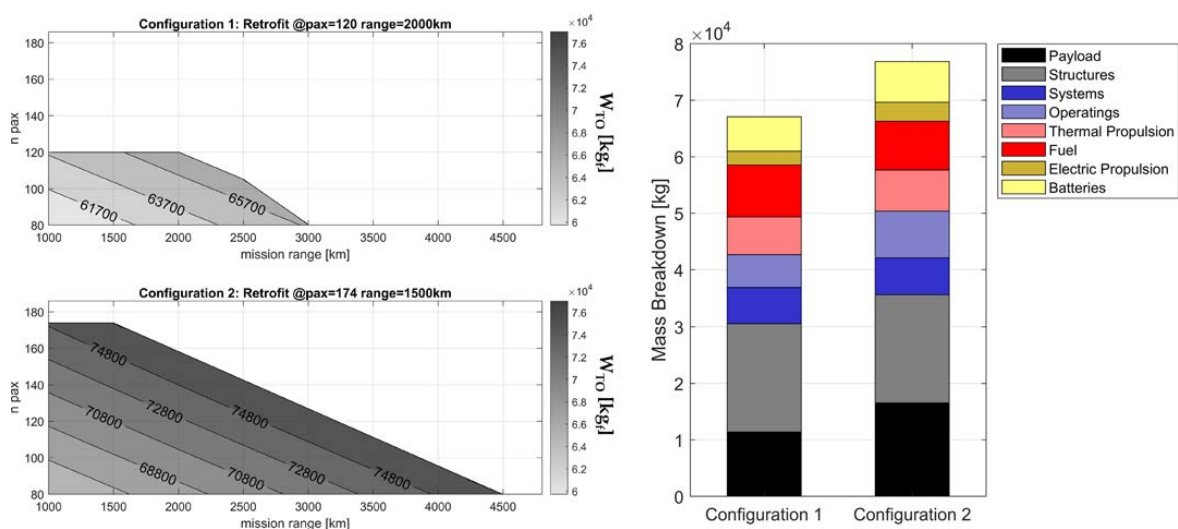


Figure 11. Take-off weight trend inside the payload-range envelope (left) and MTOW breakdown of *Configurations 1* and *2* (right).

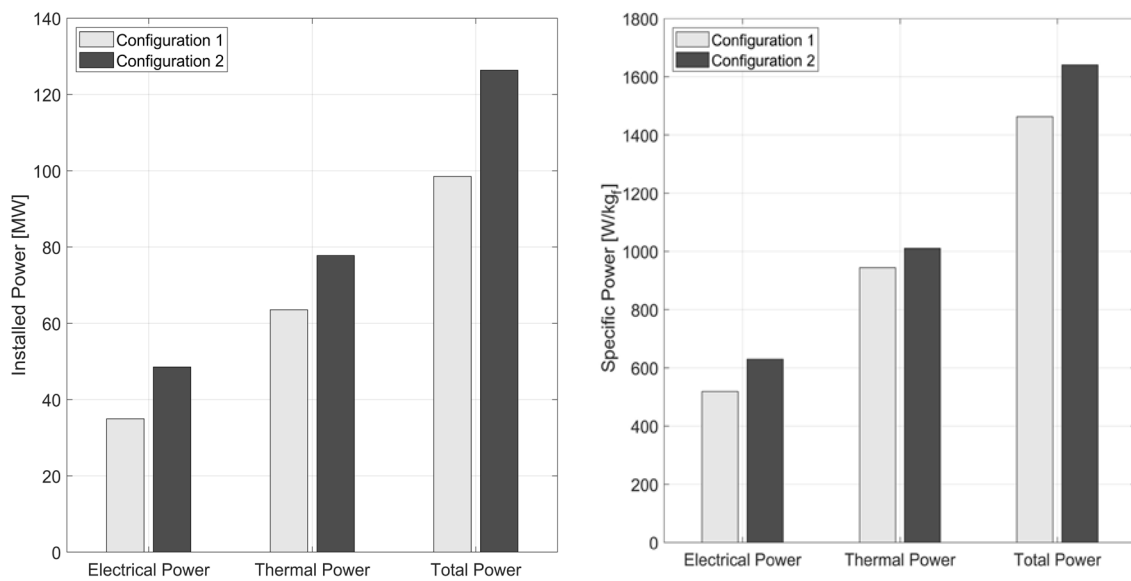


Figure 12. Installed power (left) and specific power (right).

Configuration 1 has a much more limited operational envelope than Configuration 2 due to the different choice of the design point. Being retrofitted for a smaller payload and range, in fact, Configuration 1 has a lower installed power, which constrains the operational envelope in areas where the power demand is within this limit. Configuration 2 is limited by baseline MTOW and therefore has a wider operational envelope, but, for the same payload-range pairs, shows higher battery mass and block fuel, as shown in Figure 13.

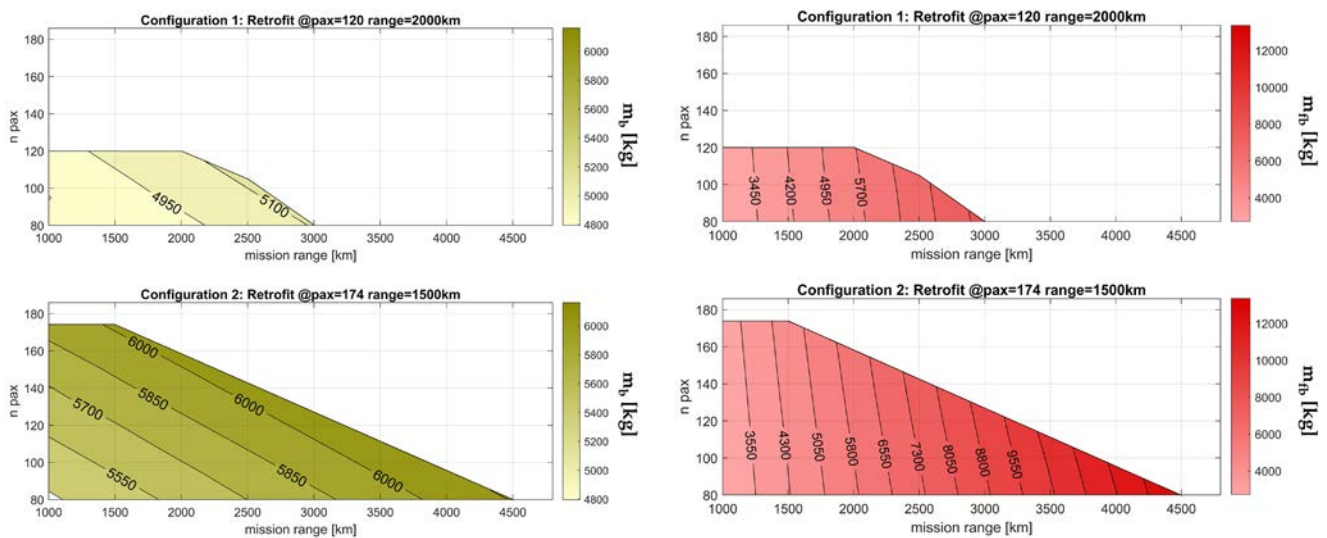


Figure 13. Battery mass (left) and block fuel mass (right).

3.4. Performance Comparison with the Baseline Aircraft

In this section, performance comparisons between the retrofitted hybrid-electric configurations and the baseline CeRAS CSR-01 are presented. In this context, Figure 9 shows the fuel consumption maps inside the payload-range envelope of the CeRAS CSR-01. To make the comparison more effective, the baseline fuel consumption is divided into LTO fuel (Figure 14a), non-LTO block fuel (Figure 14b), and the percentage of LTO fuel on the total block fuel (Figure 14c). The fuel for diversion and reserves is not included in the graphs.

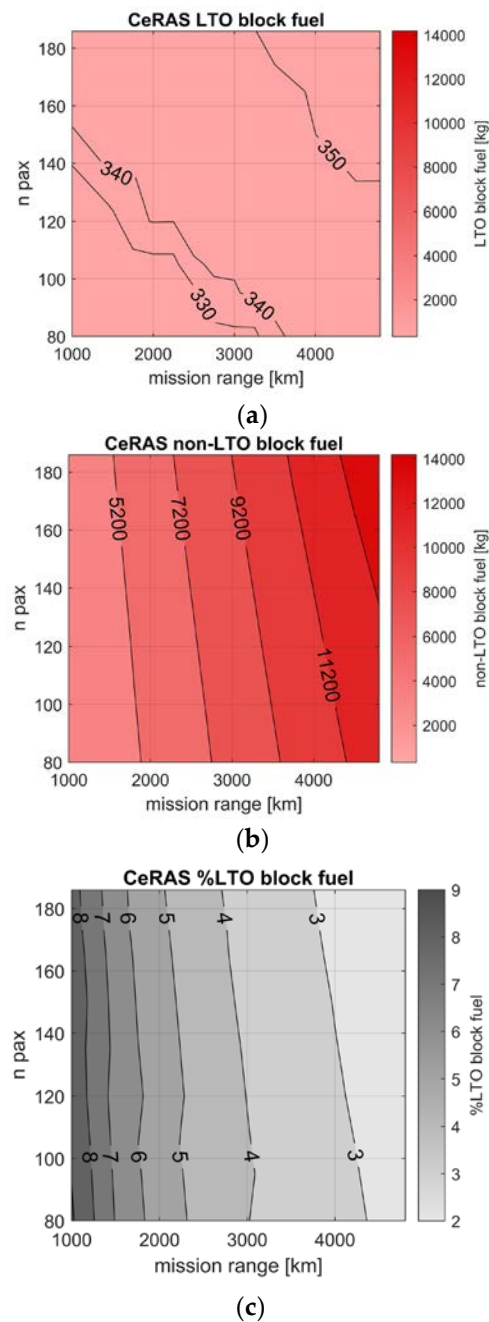


Figure 14. Block fuel of the CeRAS CSR-01: (a) LTO block fuel; (b) non-LTO block fuel; (c) Percentage contribution of LTO block fuel.

The introduction of hybrid-electric propulsion in the retrofitted configurations eliminates the fuel consumption in the LTO phase. The graphs in Figure 15 show the m_{fb} comparison between the baseline and the two hybrid-electric configurations described in Section 3.3. *Configuration 1* has a significantly smaller operational envelope than the baseline aircraft but shows a block fuel reduction for almost the entire envelope area (Figure 15-top). The reduction is more significant for low-range missions, as they are more sensitive to LTO consumption (Figure 14c). *Configuration 2* exhibits an operational envelope larger than *Configuration 1*; however, since its higher empty weight, the comparison with the baseline in terms of variation of m_{bf} fuel shows gains only for a fraction of the passenger-range envelope (Figure 15-bottom). For *Configuration 1*, the cut of pollutant emissions in the proximity of airport areas comes without penalties in block fuel in the whole operational envelope. For *Configuration 2*, instead, the m_{fb} differences become positive as the range increases.

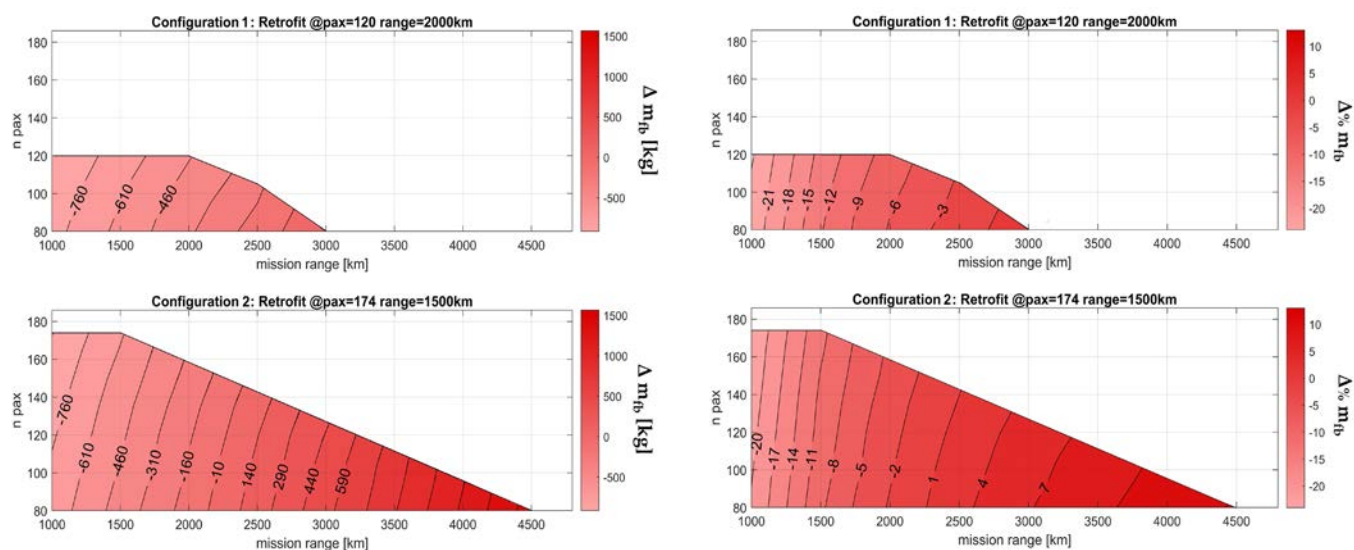


Figure 15. Total (left) and percentage (right) block fuel variations between retrofitted and baseline aircraft.

A trade-off scenario is in place: both the analysed retrofitted configurations exhibit the complete elimination of LTO direct pollutant emissions in the surroundings of airports. To achieve this, on the other hand, the two configurations must pay the price in terms of overall performance compared to the baseline: *Configuration 1* presents a significant reduction in the operational envelope, whereas it does not exhibit penalties in block fuel; *Configuration 2*, on the other hand, presents a fairly wide operating envelope, but it may show block fuel penalties, especially for longer ranges. The choice of which configuration should be further developed relies on an in-depth assessment of the pros/cons of improving the greenhouse footprint of the aircraft while reducing its operational capabilities.

4. Re-Design Strategy towards the Reduction in Greenhouse Emissions

4.1. Climate Change

Climate change is manifesting as progressive global warming. Research studying this phenomenon agrees that it is primarily influenced by the increasing greenhouse gas emissions, mainly of anthropogenic origin. To assess the contribution to climate change of an emitted substance, a metric called radiative forcing (RF) has been introduced [61]. Positive RF values indicate that the considered pollutant has a heating effect on the atmosphere. Emissions from aviation have a positive (heating) contribution to the RF [62]. The emitted substances that have the most relevant impact on RF are CO_2 , NO_x , water vapour, and soot particles [63,64]. Transport aviation currently contributes an estimated 3.5% to 4.9% of the total anthropogenic contribution to the RF [62]. Furthermore, this contribution may increase about 3–4 times by 2050 [62].

Global warming has different implications and impacts than those of local air pollution. Several studies focused on these effects on the planet and society. Although the forecasts are uncertain, ref. [65] states that even the most optimistic foresee dire scenarios for the planet; climate change will lead to the collapse of entire ecosystems, to a drastic reduction in crop productivity, with direct effects on human life. Specifically, ref. [66] predicts that agricultural production will have significant detrimental effects on growth and productivity for the 2050 scenario; the current stability of the food production system would be at risk [67]. The most food-vulnerable countries, along with areas most susceptible to flooding, drought, and rising temperatures will also be subject to dramatic migration flows [68]. Climate change will also have direct effects on human health [69] due to the increasing vulnerability to high temperatures of some categories of people and the spread of new infectious diseases.

Climate change, therefore, poses a global scale challenge; high-impact actions must be taken today to pursue a path to mitigate its catastrophic effects. Transport aviation,

therefore, must also perform its part. The solutions proposed to date mainly relate to technological improvements, such as aerodynamic refinement, development of more efficient engines, and optimisation of structures and materials to achieve weight reductions [62]. However, as the problem of aviation's impact is related to its growth, and air traffic growth forecasts seem to be much more predominant than evolutionary technological development, making improvements in little steps is no longer sufficient. It is necessary to develop and introduce completely disruptive innovations [64,70]. In this study, the integration of hybrid-electric propulsion, which has the potential to cut fuel consumption, is investigated as a solution for SMR aircraft.

4.2. Re-Design Strategy

The re-design completely differs from the retrofit procedure, both in methods and objectives. The purpose of the SMR aircraft re-design strategy is to identify possible solutions that can significantly reduce the mission fuel consumption and, therefore, greenhouse emissions with respect to the thermal baseline. In this case, THEA-CODE has been used as the objective function evaluator for the optimisation problem reported in Equation (9):

$$\begin{cases} \min(m_{fb}(x)) \\ W/S_{\min} < W/S < W/S_{\max} \\ 0 < H_P < H_{P\max} \\ 0 < \Phi_i^t < \Phi_{max}^t \end{cases} \quad (9)$$

The optimisation procedure is carried out by means of a MATLAB code; the constrained optimisation problem is solved by means of a multi-start algorithm using a sequential quadratic programming search method for local minima [71]. The objective function to be minimized is the block fuel mass m_{fb} which represents a substantial difference with the retrofit strategy. In this scenario, the optimizer can act on five design variables x_i , which are:

- W/S : aircraft wing loading; W is the design weight; and S is the wing reference area;
- H_P : degree of power hybridisation, defined as in Equation (10), where P_i^e is the electrical installed power, and P_i^t is the thermal installed power;

$$H_P = \frac{P_i^e}{P_i^e + P_i^t} \quad (10)$$

- Φ_{CL}^t : power fraction supplied by thermal engine in climb;
- Φ_{CR}^t : power fraction supplied by thermal engine in cruise;
- Φ_{DE}^t : power fraction supplied by thermal engine in descent.

The power fraction supplied by the thermal engine during the k -th phase of the mission Φ_k^t is defined in Equation (11), where P^t is the power supplied by the thermal engine during the k -th phase of the mission.

$$\Phi_k^t = \frac{P^t}{P_i^t} \quad (11)$$

From the values of Φ_k^t it is possible to also obtain the power fraction supplied by the electric motor in the k -th mission phase Φ_k^e , as the total requested power to fly is known. Indeed, the power management for a parallel hybrid-electric powertrain allows the possibility of simultaneous supply, and in different proportions, of thermal and electrical power in the climb, cruise, and descent phases. The taxiing and take-off phases, instead, are fixed and are not handled by the optimiser. Specifically, the taxiing phase is accomplished using electric power only, whereas the take-off is performed using both the available thermal and electric power. The diversion needs to be taken into account for sizing, but since it is not performed in standard operations, its emissions do not have a significant overall impact. For this reason, it has been decided to accomplish the whole diversion with thermal power only. This avoids the need to carry a larger amount of batteries, which would increase the empty weight of the aircraft, reducing the achievable operating performance without any practical

advantages in terms of environmental impact. Figure 16 schematically summarises the power management strategy along with the full mission for the re-design procedure.

mission phase	power utilization strategy
taxi-out	full electric
take-off	electric + thermal
climb	electric + thermal
cruise	electric + thermal
descent	electric + thermal
diversion	full thermal
loiter	full thermal
landing	full thermal
taxi-in	full electric

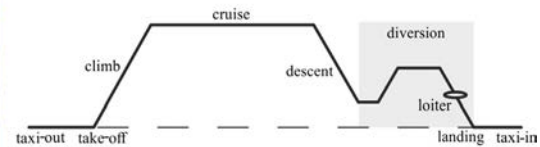


Figure 16. Qualitative power split supply strategy for the design procedure.

Differently from the retrofitting procedure, in which the aircraft shape is kept frozen, in the re-design, the lifting system is designed for each configuration evaluated; furthermore, the weight of each component is computed for each configuration assessed.

The wing loading, which is of primary relevance to define the matching chart and thus to size the propulsion system in accordance with the selected H_P , has also been used to re-scale the geometry of each configuration evaluated during the optimisation. Indeed, to avoid increasing the complexity of the procedure by also introducing the geometrical parameters of the wing as design variables, the geometry of the baseline aircraft has been homothetically scaled (Figure 17) by using the wing loading as a scaling factor.

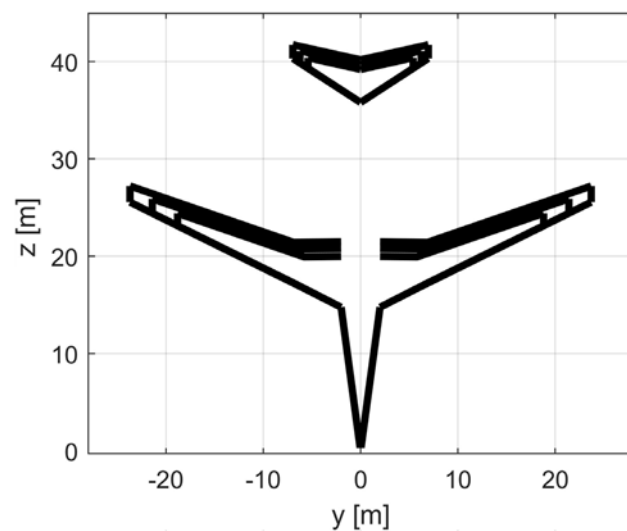


Figure 17. Example of scaled geometries.

4.3. Re-Design Results

In this section, the results of the re-design of hybrid-electric SMR aircraft are reported and discussed. To obtain a sufficiently detailed overview at this conceptual stage, different optimisations have been performed by varying TLAR. Specifically, configurations with a number of passengers of 115, 150, and 185, and design routes lengths of 1000, 2000, 3000, and 4000 km have been considered, respectively. In order to evaluate only configurations with effective integration of a quota of electric propulsion, the design variable H_P has been set strictly larger than zero ($H_P > 0$). Additional cases with $H_P = 0$, i.e., SMR aircraft with only thermal power, have been performed with the same design methodology for

each payload-range pair, and the related results have been used to make performance comparisons with the corresponding hybrid-electric configurations.

A general comparison between the outcomes of the optimal hybrid-electric configurations and the thermal ones is proposed; Figure 18 shows the percentage (left) and absolute (right) differences of MTOW and m_{fb} . From Figure 18-left, it emerges that the integration of hybrid propulsion on this class of aircraft does not lead to any block fuel reduction for each payload and range considered. Hybrid-electric optima solutions exhibit significant increases in the MTOW. The penalisation in block fuel rapidly increase as the design range increases, for each payload considered, reaching an increase in m_{fb} up to 24% when the design range reaches 4000 km. These conceptual results highlight that, with the current forecast on the battery technology level, introducing hybrid-electric propulsion in medium-range aircraft does not provide advantages; indeed, it provides increases in fuel consumption with respect to a conventional thermal competitor if typical medium-haul routes are considered.

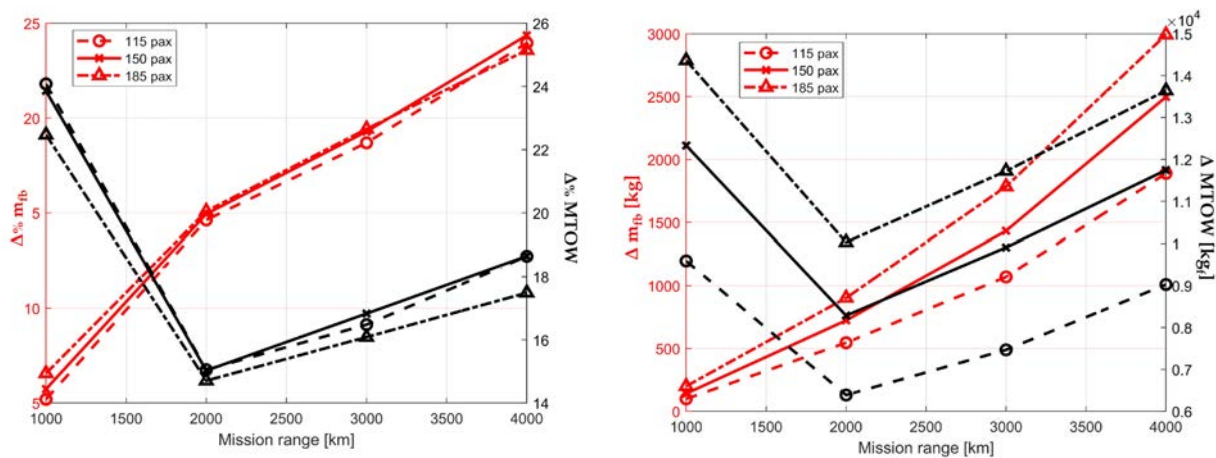


Figure 18. MTOW and block fuel comparison between the hybrid-electric and the full-thermal configurations: percentage (left), absolute (right).

Figure 19 shows the outcomes of the optimisation related to the power supply strategy for climb, cruise, and descent, respectively; the case of 115 passengers' configurations is taken as a general example. The optimiser finds optima solutions which exhibit almost zero electric power supply in cruise. Since this phase is the most energy demanding, using electric power in cruise would result in such detrimental weight increases that there would be no benefit in terms of block fuel reduction. Apart from the share of electrical energy required for ground operations (that are not design variables, see Section 4.2), the optimiser finds solutions in which electric power is partially used only in climb; the descent is marginally relevant in the overall power breakdown.

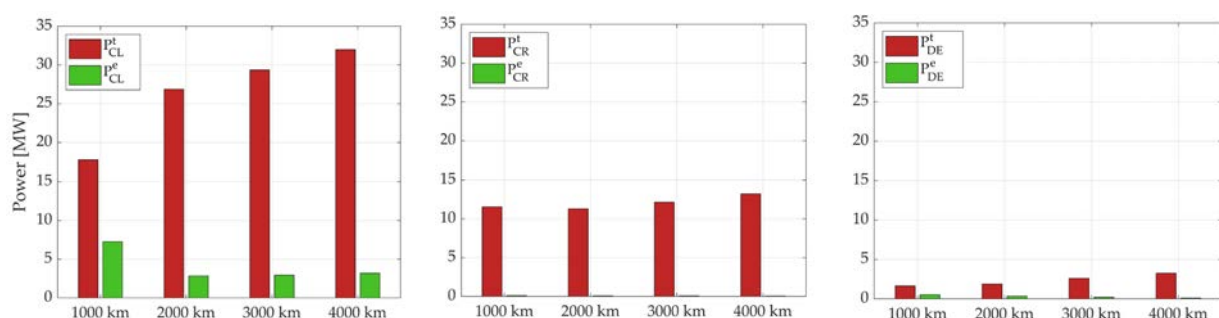


Figure 19. Thermal and electric power supplied in climb (left), cruise (centre), and descent (right) for configurations with 115 passengers.

5. Conclusions

In this paper, the conceptual study of the integration of hybrid-electric propulsion on a short-medium range transport aircraft has been addressed. The main purpose of this study is to evaluate the impact of hybrid-electric propulsion on the mitigation of the environmental impact of transport aviation. The results obtained provide different outcomes if local air quality and climate change issues are considered. On one side, hybrid-electric propulsion appears as an effective solution to tackle the problem of the degradation of air quality in airport areas. This problem is related to the pollutant emissions produced by aircraft during taxiing, take-off, climb-out, and approach (LTO cycle) and can be eliminated through the proper integration of a share of electrical power on board. Specifically, the electrical powertrain must be sized to meet the power required for the LTO cycle, whereas thermal power is used in the other phases. In this way, the use of thermal engines in areas close to the ground is avoided, and pollutant emissions that deteriorate local air quality are suppressed. However, contractions of aircraft operating envelope must be taken into account, both in terms of reduction in payload weight and design range. Changing viewpoint, hybrid-electric propulsion does not emerge as an effective solution for reducing overall fuel consumption of medium-range aircraft and thus seems to have no potential for mitigating the climate-changing impact of transport aviation. Specifically, no savings in fuel consumption have been found in any operating scenario, while conversely, severe penalties in take-off weight and fuel consumption are obtained for the relevant flight ranges of the considered aircraft category. This result is mainly attributed to the low energy density of batteries, even considering the technological levels forecasted for the next decade.

This study, hence, indicates that alternative solutions to hybrid-electric propulsion must be explored to address the impact of transport aviation on climate change. New energy sources or new propulsion technologies capable of drastically reducing greenhouse emissions must be developed for SMR aircraft class. On the other hand, the problem of local air quality in airport areas seems to be addressable with the use of electric power, although an increase in the detail of the study of this integration is necessary. Indeed, a potential advancement in this investigation may lie in the detailing of the integration of electrical power systems into current turbofan architectures; this is a complex engineering problem and requires in-depth studies. Following this phase, the assessment of the noise levels generated during the LTO cycle should be addressed in order to quantify the possible benefits of supplying electric power only.

Finally, to achieve benefits in the whole operating mission for a short-medium range aircraft, a different concept for hybrid propulsion can be supposed; the benefits of electric propulsion can be exploited for LTO operations, whereas thermal engines fed by sustainable aviation fuels or liquid hydrogen may have the potential to significantly reduce greenhouse emissions.

Author Contributions: Conceptualization, K.A.S. and G.P.; methodology and software, K.A.S. and G.P.; validation, K.A.S., G.P., A.A.Q. and M.R.C.; formal analysis and investigation, K.A.S. and G.P.; resources, A.A.Q. and M.R.C.; data curation, K.A.S. and G.P.; writing—original draft preparation, K.A.S. and G.P.; writing—review and editing and visualisation, K.A.S., G.P., A.A.Q. and M.R.C.; supervision and project administration, M.R.C. All authors have read and agreed to the published version of the manuscript.

Funding: This research received no external funding.

Data Availability Statement: The data presented in this study are available on request from the corresponding author.

Conflicts of Interest: The authors declare no conflict of interest.

List of Symbols and Abbreviations

Symbol	Description	Unit
C_D	Aircraft drag coefficient	-
C_L	Aircraft lift coefficient	-
C_{Lmax}	Maximum lift coefficient	-
C_t	Thrust specific fuel consumption	1/s
D	Aircraft drag	N
g	Gravitational acceleration	m/s ²
H_P	Degree of power hybridization	-
k_e	One engine inoperative factor	-
k_{V2}	Take-off final speed—stall speed ratio	-
k_{VA}	Approach speed—stall speed ratio	-
k_{VR}	Rotation speed—stall speed ratio	-
k_{VT}	Touch down speed—stall speed ratio	-
m_b	Battery mass	kg
m_{fb}	Block fuel mass	kg
L	Aircraft lift	N
l_{TO}	Balanced field length	m
P	Power request to fly	W
P/W	Specific power	W/N
P_b	Power supplied by the battery pack	W
P_i^e	Installed electric motor power	W
P^t	Power supplied by thermal engine	W
P_i^t	Installed thermal engine power	W
q	Dynamic pressure	Pa
R_N	Vertical ground reaction force	N
R_T	Horizontal ground reaction force	N
S	Wing reference area	m ²
S_{LO}	Distance covered during lift-off	m
S_R	Distance covered during rotation	m
T	Engine thrust	N
V	Aircraft true air speed	m/s
W	Aircraft weight	N
W_{TO}	Aircraft take-off weight	N
W/S	Wing loading	N/m ²
γ	Trajectory slope	rad
η_{ec}	Electric chain efficiency	-
η_p	Propulsive efficiency	-
η_{tc}	Thermal chain efficiency	-
μ_{TO}	Friction coefficient during ground roll	-
ρ	Air density	kg/m ³
φ	Take-off distance safety factor	-
ϕ^e	Power fraction supplied by the electric motor	-
ϕ^t	Power fraction supplied by the thermal engine	-

Abbreviations

AVL	Athena Vortex Lattice
BED	Gravimetric battery energy density
CeRAS	Central reference aircraft data system
LTO	Landing and take-off cycle
MTOW	Maximum take-off weight
PM	Particulate matter
RF	Radiative forcing
SMR	Short-medium range
THEA-CODE	Tool for hybrid-electric aircraft conceptual design
TLAR	Top level aircraft requirements
VLM	Vortex Lattice Method
VOC	Volatile organic compounds

Appendix A

In this Section, a summary of the rationale of Equations (1)–(4) is detailed.

Take-off constraint—Equation (1)

The take-off run can be split in three parts, namely, ground roll, rotation, and lift-off. During the ground roll, the aircraft attitude does not change, and the engine thrust is set to the maximum value; once the rotation speed is reached, the elevator is deflected, and the aircraft rotates around the main landing gear; the lift-off phase starts when the aircraft pulls the wheels off the ground. The take-off field length has been derived according to the following hypothesis: (i) the aircraft has been considered as a point mass; (ii) no ground effect aerodynamics has been taken into account; and (iii) no engine failure has been considered. In the ground roll phase, there are different forces acting on the aircraft, namely lift, drag, engine thrust, and ground reaction forces (R_N , R_T). The aircraft motion can be described, in terms of power, by Equation (A1):

$$\eta_P P - DV - \mu_{TO} V(W - L) = \frac{W}{g} V^2 \frac{dV}{ds} \quad (\text{A1})$$

Considering the well-known relationship of lift and drag, and assuming a linear relationship between propulsive efficiency η_P and the aircraft speed, the ground roll distance (S_{GR}) can be obtained as in Equation (A2).

$$S_{GR} = -\frac{\frac{W}{S}}{g\rho(C_D - \mu_{TO}C_L)} \log \left(1 - \frac{k_{V_R}^2 (C_D - \mu_{TO}C_L)}{\left(\frac{\eta_P}{V_2} \left(\frac{P}{W}\right) - \mu_{TO}\right) C_{Lmax}} \right) \quad (\text{A2})$$

During rotation phase, the distance covered by the aircraft can be calculated assuming a constant speed equal to the rotation speed V_R , so the covered distance in this phase is calculated according to Equation (A3); t_R is the duration of this phase.

$$S_R = V_R t_R \quad (\text{A3})$$

During lift-off phase, the aircraft pulls the wheel off the ground, and its path can be approximated by a circular trajectory, so Equation (A4) can be used to evaluate the covered horizontal distance; h is the obstacle height and is equal to 35 ft.

$$S_{LO} = R \sqrt{1 - \left(1 - \frac{h}{R}\right)^2} \quad (\text{A4})$$

Combining Equations (A2)–(A4), the take-off field length S_{TO} is given by Equation (A5).

$$S_{TO} = S_{GR} + S_R + S_{LO} \quad (\text{A5})$$

S_{TO} must be lower than the balanced field length l_{TO} set by the TLARs, so inequality (A6) should be verified; φ is a security factor which has been set equal to 1.15.

$$S_{TO} \leq \frac{l_{TO}}{\varphi} \quad (\text{A6})$$

By substituting Equations (A2)–(A5) in inequality (A6), the relationship between wing loading and specific power during take-off phase can be obtained, as reported in Equation (A7).

$$\left(\frac{P}{W}\right)_{TO} \geq \left(\mu_{TO} + \frac{k_{VR}^2 (C_D - \mu_{TO} C_L)}{C_{L,max}} \right) \sqrt{\frac{2(W/S) k_{V2}}{\rho C_{L,max} \eta_p}} \quad (\text{A7})$$

Climb and obstacle limitations—Equation (2)

According to FAR 25.115, if an engine failure occurs after the decisional speed, the aircraft must take-off and guarantee a minimum flight trajectory slope. The aircraft trajectory, also called take-off flight path, can be divided into four segments; for each segment, a minimum slope is fixed by regulations according to the number of available engines. In the case of hybrid-electric propulsion, the intrinsic redundancy due to the presence of two different power sources increases the aircraft reliability. On the other hand, the power allocation to each subsystem (i.e., thermal engine and electric motor) could be not trivial from a redundancy perspective, and it is strictly dependent on the architecture and sizing of hybrid-electric powertrain; for example, in the case of two or more powertrains, different combinations of failures could occur. To simplify the analysis, the following assumption has been considered: if a failure occurs, the propulsor cannot be fed by both thermal engine and electric motor; this assumption can be considered as conservative. To compute the requested power in this mission phase, the following assumptions have been considered: (i) the aircraft has been considered a point mass; and (ii) the climb is steady. According to the previous hypotheses, the aircraft trim in the i -th phase of the *take-off flight path*, is defined by Equation (A8):

$$\begin{cases} \gamma_i = \frac{T - D_i}{W} \\ k_e P_i \eta_p = TV_i \end{cases} \quad (\text{A8})$$

where, k_e is the one engine inoperative factor, and it is defined by the current regulations [38]. By rearranging the previous equations and imposing that the trajectory slope must be higher than the value γ_i imposed by regulations, inequality (A9) can be derived.

$$\left(\frac{P}{W}\right)_{CL_i} \geq \frac{\left(\frac{q C_{Di} V_i}{W S} + \gamma_i V_i\right)}{k_e \eta_p} \quad (\text{A9})$$

Cruise—Equation (3)

The cruise Mach number and altitude are selected according to the TLARs. The assumptions to assess the specific power of this phase are equal to the ones of the climb phase, so the specific power can be calculated by imposing the trajectory slope equal to zero.

Aborted landing—Equation (4)

Aborted landing requirements are defined in FAR 25.119; according to these requirements, the specific power can be calculated assuming the same hypotheses of the climb phase.

References

1. Brooker, P. Civil aircraft design priorities: Air quality? climate change? noise? *Aeronaut. J.* **2006**, *110*, 517–532. [[CrossRef](#)]
2. Stettler, M.E.J.; Eastham, S.; Barrett, S.R.H. Air quality and public health impacts of UK airports. Part I: Emissions. *Atmos. Environ.* **2011**, *45*, 5415–5424. [[CrossRef](#)]
3. Parker, R. From blue skies to green skies: Engine technology to reduce the climate-change impacts of aviation. *Technol. Anal. Strat. Manag.* **2009**, *21*, 61–78. [[CrossRef](#)]

4. ICAO. Local Air Quality Technology Standards. 2017. Available online: https://www.icao.int/environmental-protection/Pages/LAQ_TechnologyStandards.aspx (accessed on 18 April 2023).
5. Brelje, B.J.; Martins, J.R. Electric, hybrid, and turboelectric fixed-wing aircraft: A review of concepts, models, and design approaches. *Prog. Aerosp. Sci.* **2018**, *104*, 1–19. [[CrossRef](#)]
6. Abu Salem, K.; Palaia, G.; Quarta, A.A. Review of hybrid-electric aircraft technologies and designs: Critical analysis and novel solutions. *Prog. Aerosp. Sci.* **2023**; *under review*.
7. Zhao, L.; Lakraychi, A.E.; Chen, Z.; Liang, Y.; Yao, Y. Roadmap of Solid-State Lithium-Organic Batteries toward 500 Wh kg⁻¹. *ACS Energy Lett.* **2021**, *6*, 3287–3306. [[CrossRef](#)]
8. Riboldi, C.; Gualdoni, F. An integrated approach to the preliminary weight sizing of small electric aircraft. *Aerosp. Sci. Technol.* **2016**, *58*, 134–149. [[CrossRef](#)]
9. Finger, D.F.; Bil, C.; Braun, C. Initial Sizing Methodology for Hybrid-Electric General Aviation Aircraft. *J. Aircr.* **2020**, *57*, 245–255. [[CrossRef](#)]
10. Isikveren, A.T.; Fefermann, Y.; Maury, C.; Level, C.; Zarati, K.; Salanne, J.-P.; Pornet, C.; Thoraval, B. Pre-design of a commuter transport utilising Voltaic-Joule/Brayton motive power systems. *Aeronaut. J.* **2017**, *122*, 205–237. [[CrossRef](#)]
11. Orefice, F.; Nicolosi, F.; Della Vecchia, P.; Ciliberti, D. Aircraft Conceptual Design of Commuter Aircraft including Distributed Electric Propulsion. In Proceedings of the AIAA Aviation 2020 Forum, Virtual, 15–19 June 2020. [[CrossRef](#)]
12. Rolando, A.; Salucci, F.; Trainelli, L.; Riboldi, C.E.; Khan, Y.M. On the Design of an Electric-Powered Micro-Feeder Aircraft. In Proceedings of the 1st Aerospace Europe Conference, Bordeaux, France, 25–28 February 2020.
13. Palaia, G.; Abu Salem, K.; Cipolla, V.; Binante, V.; Zanetti, D. A Conceptual Design Methodology for e-VTOL Aircraft for Urban Air Mobility. *Appl. Sci.* **2021**, *11*, 10815. [[CrossRef](#)]
14. Donato, T.; Ficarella, A. A Methodology for the Comparative Analysis of Hybrid Electric and All-Electric Power Systems for Urban Air Mobility. *Energies* **2022**, *15*, 638. [[CrossRef](#)]
15. Voskuil, M.; van Bogaert, J.; Rao, A.G. Analysis and design of hybrid electric regional turboprop aircraft. *CEAS Aeronaut. J.* **2017**, *9*, 15–25. [[CrossRef](#)]
16. Palaia, G.; Abu Salem, K. Mission Performance Analysis of Hybrid-Electric Regional Aircraft. *Aerospace* **2023**, *10*, 246. [[CrossRef](#)]
17. Hoelzen, J.; Liu, Y.; Bensmann, B.; Winnefeld, C.; Elham, A.; Friedrichs, J.; Hanke-Rauschenbach, R. Conceptual Design of Operation Strategies for Hybrid Electric Aircraft. *Energies* **2018**, *11*, 217. [[CrossRef](#)]
18. De Vries, R.; Brown, M.; Vos, R. Preliminary Sizing Method for Hybrid-Electric Distributed-Propulsion Aircraft. *J. Aircr.* **2019**, *56*, 2172–2188. [[CrossRef](#)]
19. Palaia, G. Design and Performance Assessment Methodologies for Box-Wing Hybrid-Electric Aircraft from Urban to Regional Transport Applications. Ph.D. Thesis, University of Pisa, Pisa, Italy, 2022. Available online: <https://etd.adm.unipi.it/t/etd-1109-2022-150110/> (accessed on 18 April 2023).
20. Airbus. Global Market Forecast 2021–2040. 2022. Available online: <https://www.airbus.com/en/products-services/commercial-aircraft/market/global-market-forecast> (accessed on 18 April 2023).
21. Graver, B.; Zhang, K.; Rutherford, D. CO₂ emissions from commercial aviation. In *The International Council on Clean Transportation*; ICCT: Washington, DC, USA, 2018. Available online: <https://theicct.org/publications/co2-emissions-commercial-aviation-2018> (accessed on 18 April 2023).
22. Pornet, C.; Isikveren, A. Conceptual design of hybrid-electric transport aircraft. *Prog. Aerosp. Sci.* **2015**, *79*, 114–135. [[CrossRef](#)]
23. Gnadt, A.R.; Speth, R.L.; Sabnis, J.S.; Barrett, S.R. Technical and environmental assessment of all-electric 180-passenger commercial aircraft. *Prog. Aerosp. Sci.* **2018**, *105*, 1–30. [[CrossRef](#)]
24. Sgueglia, A.; Schmollgruber, P.; Bartoli, N.; Benard, E.; Morlier, J.; Jasa, J.; Martins, J.R.R.A.; Hwang, J.T.; Gray, J.S. Multidisciplinary Design Optimization Framework with Coupled Derivative Computation for Hybrid Aircraft. *J. Aircr.* **2020**, *57*, 715–729. [[CrossRef](#)]
25. Risse, K.; Schäfer, K.; Schültke, F.; Stumpf, E. Central Reference Aircraft data System (CeRAS) for research community. *CEAS Aeronaut. J.* **2015**, *7*, 121–133. [[CrossRef](#)]
26. CeRAS. Central Reference Aircraft System. Website. 2016. Available online: <https://ceras.ilr.rwth-aachen.de/> (accessed on 18 April 2023).
27. Abu Salem, K.; Cipolla, V.; Palaia, G.; Binante, V.; Zanetti, D. A Physics-Based Multidisciplinary Approach for the Preliminary Design and Performance Analysis of a Medium Range Aircraft with Box-Wing Architecture. *Aerospace* **2021**, *8*, 292. [[CrossRef](#)]
28. Palaia, G.; Zanetti, D.; Abu Salem, K.; Cipolla, V.; Binante, V. THEA-CODE: A design tool for the conceptual design of hybrid-electric aircraft with conventional or unconventional airframe configurations. *Mech. Ind.* **2021**, *22*, 19. [[CrossRef](#)]
29. Drela, M.; Youngren, H. AVL 3.36 User Primer, Online Software Manual. 2017. Available online: <https://perma.cc/R35R-W29F> (accessed on 18 April 2023).
30. Raymer, P. *Aircraft Design: A Conceptual Approach*; AIAA Education Series; American Institute of Aeronautics and Astronautics Inc.: Reston, VA, USA, 1992; ISBN 0-930403-51-7.
31. Mason, W. Analytic models for technology integration in aircraft design. In Proceedings of the Aircraft Design, Systems and Operations Conference, Dayton, OH, USA, 17–19 September 1990. [[CrossRef](#)]
32. Gu, X.; Ciampa, P.D.; Nagel, B. An automated CFD analysis workflow in overall aircraft design applications. *CEAS Aeronaut. J.* **2017**, *9*, 3–13. [[CrossRef](#)]

33. Wang, Z.J. High-order computational fluid dynamics tools for aircraft design. *Philos. Trans. R. Soc. A Math. Phys. Eng. Sci.* **2014**, *372*, 20130318. [[CrossRef](#)] [[PubMed](#)]
34. Da Ronch, A.; Ghoreysi, M.; Badcock, K. On the generation of flight dynamics aerodynamic tables by computational fluid dynamics. *Prog. Aerosp. Sci.* **2011**, *47*, 597–620. [[CrossRef](#)]
35. Carini, M.; Meheut, M.; Kanellopoulos, S.; Cipolla, V.; Abu Salem, K. Aerodynamic analysis and optimization of a boxwing architecture for commercial airplanes. In Proceedings of the AIAA Scitech 2020 Forum, Orlando, FL, USA, 6–10 January 2020. [[CrossRef](#)]
36. Fioriti, M. Adaptable conceptual aircraft design model. *Adv. Aircr. Spacecr. Sci.* **2014**, *1*, 43–67. [[CrossRef](#)]
37. Sforza, P.M. *Commercial Airplane Design Principles*; Elsevier: Amsterdam, The Netherlands, 2014.
38. FAR 25; Airworthiness Standards: Transport Category Airplanes. FAA: Washington, DC, USA, 1980.
39. Mair, W.A.; Birdsall, D.L. *Aircraft Performance*; Cambridge University Press: Cambridge, UK, 1992. [[CrossRef](#)]
40. Airbus. Getting to Grips with Aircraft Performance, Airbus SAS. 2002. Available online: <https://perma.cc/FQ9P-FET4> (accessed on 18 April 2023).
41. Abu Salem, K. Development of Design Tools and Methods for Box-Wing Airplanes and Application of the PrandtlPlane Concept to a Short-Medium Range Aircraft. Ph.D. Thesis, University of Pisa, Pisa, Italy, 2021. Available online: <https://etd.adm.unipi.it/theses/available/etd-05312021-171241/> (accessed on 18 April 2023).
42. Wells, D.; Horvath, B.; McCullers, L. The Flight Optimization System Weights Estimation Method. NASA Technical Memorandum; No. 2017-219627. 2017. Available online: <https://ntrs.nasa.gov/citations/20170005851> (accessed on 18 April 2023).
43. Abu Salem, K.; Giuseppe, P.; Vittorio, C.; Vincenzo, B.; Davide, Z.; Mario, C. Tools and methodologies for box-wing aircraft conceptual aerodynamic design and aeromechanic analysis. *Mech. Ind.* **2021**, *22*, 39. [[CrossRef](#)]
44. Seitz, A.; Nickl, M.; Stroh, A.; Vratny, P.C. Conceptual study of a mechanically integrated parallel hybrid electric turbofan. *Proc. Inst. Mech. Eng. Part G J. Aerosp. Eng.* **2018**, *232*, 2688–2712. [[CrossRef](#)]
45. Dever, T.P.; Duffy, K.P.; Provenza, A.J.; Loyselle, P.L.; Choi, B.B.; Morrison, C.R.; Lowe, A.M. Assessment of Technologies for Noncryogenic Hybrid Electric Propulsion; Report NASA TP-2015-216588. 2015. Available online: <https://ntrs.nasa.gov/citations/20150000747> (accessed on 18 April 2023).
46. ICAO. *Global Air Transport Outlook to 2030 and Trends to 2040*; ICAO: Rio de Janeiro, Brazil, 2013.
47. Eurocontrol. European Aviation in 2040, Challenges of Growth, Annex 1, Flight Forecast to 2040. 2018. Available online: <https://perma.cc/YW6Y-JU7J> (accessed on 18 April 2023).
48. Eurocontrol. European Aviation in 2040, Challenges of Growth. 2018. Available online: <https://perma.cc/2A2J-B7PW> (accessed on 18 April 2023).
49. Yang, X.; Cheng, S.; Lang, J.; Xu, R.; Lv, Z. Characterization of aircraft emissions and air quality impacts of an international airport. *J. Environ. Sci.* **2018**, *72*, 198–207. [[CrossRef](#)]
50. Rissman, J.; Arunachalam, S.; Woody, M.; West, J.J.; BenDor, T.; Binkowski, F.S. A plume-in-grid approach to characterize air quality impacts of aircraft emissions at the Hartsfield–Jackson Atlanta International Airport. *Atmos. Chem. Phys.* **2013**, *13*, 9285–9302. [[CrossRef](#)]
51. Hudda, N.; Durant, L.W.; Fruin, S.A.; Durant, J.L. Impacts of Aviation Emissions on Near-Airport Residential Air Quality. *Environ. Sci. Technol.* **2020**, *54*, 8580–8588. [[CrossRef](#)]
52. Simonetti, I.; Maltagliati, S.; Manfrida, G. Air quality impact of a middle size airport within an urban context through EDMS simulation. *Transp. Res. Part D Transp. Environ.* **2015**, *40*, 144–154. [[CrossRef](#)]
53. Zhu, Y.; Fanning, E.; Yu, R.C.; Zhang, Q.; Froines, J.R. Aircraft emissions and local air quality impacts from takeoff activities at a large International Airport. *Atmos. Environ.* **2011**, *45*, 6526–6533. [[CrossRef](#)]
54. Winther, M.; Kousgaard, U.; Ellermann, T.; Massling, A.; Nøjgaard, J.K.; Ketzel, M. Emissions of NO_x, particle mass and particle numbers from aircraft main engines, APU's and handling equipment at Copenhagen Airport. *Atmos. Environ.* **2015**, *100*, 218–229. [[CrossRef](#)]
55. Yim, S.H.; Stettler, M.E.; Barrett, S.R. Air quality and public health impacts of UK airports. Part II: Impacts and policy assessment. *Atmos. Environ.* **2013**, *67*, 184–192. [[CrossRef](#)]
56. Aircraft air pollutant emissions in Greek airports. *Glob. NEST Int. J.* **2013**, *11*, 528–534. [[CrossRef](#)]
57. Vratny, P.C.; Kling, U. *Impact of Electric Taxiing on Hybrid-Electric Aircraft Sizing*; Deutsche Gesellschaft für Luft-und Raumfahrt-Lilienthal-Oberth eV: Bonn, Germany, 2019.
58. Pornet, C.; Gologan, C.; Vratny, P.C.; Seitz, A.; Schmitz, O.; Isikveren, A.T.; Hornung, M. Methodology for Sizing and Performance Assessment of Hybrid Energy Aircraft. *J. Aircr.* **2015**, *52*, 341–352. [[CrossRef](#)]
59. Ang, A.W.X.; Rao, A.G.; Kanakis, T.; Lammen, W. Performance analysis of an electrically assisted propulsion system for a short-range civil aircraft. *Proc. Inst. Mech. Eng. Part G J. Aerosp. Eng.* **2018**, *233*, 1490–1502. [[CrossRef](#)]
60. Gesell, H.; Wolters, F.; Plohr, M. System analysis of turbo-electric and hybrid-electric propulsion systems on a regional aircraft. *Aeronaut. J.* **2019**, *123*, 1602–1617. [[CrossRef](#)]
61. Shine, K.P.; Derwent, R.G.; Wuebbles, D.J.; Morcrette, J.J. Radiative forcing of climate. In *Climate Change: The IPCC Scientific Assessment*; 1990; pp. 41–68. Available online: https://pure.mpg.de/rest/items/item_3475154/component/file_3475155/content (accessed on 18 April 2023).

62. Lee, D.S.; Fahey, D.W.; Forster, P.M.; Newton, P.J.; Wit, R.C.N.; Lim, L.L.; Owen, B.; Sausen, R. Aviation and global climate change in the 21st century. *Atmos. Environ.* **2009**, *43*, 3520–3537. [[CrossRef](#)]
63. Lee, D.; Pitari, G.; Grewe, V.; Gierens, K.; Penner, J.; Petzold, A.; Prather, M.; Schumann, U.; Bais, A.; Berntsen, T. Transport impacts on atmosphere and climate: Aviation. *Atmos. Environ.* **2010**, *44*, 4678–4734. [[CrossRef](#)]
64. Ribeiro, S.K.; Kobayashi, S.; Beuthe, M.; Gasca, J.; Greene, D.; Lee, D.S.; Muromachi, Y.; Newton, P.J.; Plotkin, S.; Sperling, D.; et al. Transportation and its Infrastructure. UC Davis: Institute of Transportation Studies. 2007. Available online: <https://escholarship.org/uc/item/98m5t1rv> (accessed on 18 April 2023).
65. McNutt, M. Climate Change Impacts. *Science* **2013**, *341*, 435. [[CrossRef](#)] [[PubMed](#)]
66. Calzadilla, A.; Rehdanz, K.; Betts, R.; Falloon, P.; Wiltshire, A.; Tol, R. Climate change impacts on global agriculture. *Clim. Change* **2013**, *120*, 357–374. [[CrossRef](#)]
67. Wheeler, T.; Von Braun, J. Climate Change Impacts on Global Food Security. *Science* **2013**, *341*, 508–511. [[CrossRef](#)] [[PubMed](#)]
68. Kaczan, D.J.; Orgill-Meyer, J. The impact of climate change on migration: A synthesis of recent empirical insights. *Clim. Change* **2019**, *158*, 281–300. [[CrossRef](#)]
69. Haines, A.; Patz, J.A. Health Effects of Climate Change. *JAMA* **2004**, *291*, 99. [[CrossRef](#)]
70. Tasca, A.L.; Cipolla, V.; Abu Salem, K.; Puccini, M. Innovative Box-Wing Aircraft: Emissions and Climate Change. *Sustainability* **2021**, *13*, 3282. [[CrossRef](#)]
71. Fletcher, R. *Practical Methods of Optimization*; John Wiley & Sons: Hoboken, NJ, USA, 2013; ISBN 978-1-118-72318-0.

Disclaimer/Publisher’s Note: The statements, opinions and data contained in all publications are solely those of the individual author(s) and contributor(s) and not of MDPI and/or the editor(s). MDPI and/or the editor(s) disclaim responsibility for any injury to people or property resulting from any ideas, methods, instructions or products referred to in the content.